J. Membrane Biol. 194, 153–164 (2003)
DOI: 10.1007/s00232-003-2035-7

The Journal of
Membrane
Biology

Syntaxin Is Efficiently Excluded from Sphingomyelin-enriched Domains in Supported Lipid Bilayers Containing Cholesterol

D.E. Saslowsky, J.C. Lawrence, R.M. Henderson, J.M. Edwardson
Department of Pharmacology, University of Cambridge, Tennis Court Road, Cambridge CB2 1PD, United Kingdom

Received: 8 January 2003/Revised 16 April 2003

Abstract. Formation of a *trans*-complex between the three SNARE proteins syntaxin, synaptobrevin and SNAP-25 drives membrane fusion. The structure of the core SNARE complex has been studied extensively. Here we have used atomic force microscopy to study the behavior of recombinant syntaxin 1A both in detergent extracts and in a lipid environment. Full-length syntaxin in detergent extracts had a marked tendency to aggregate, which was countered by addition of munc-18. In contrast, syntaxin lacking its transmembrane region was predominantly monomeric. Syntaxin could be integrated into liposomes, which formed lipid bilayers when deposited on a mica support. Supported bilayers were decorated with lipid vesicles in the presence, but not the absence, of full-length syntaxin, indicating that formation of syntaxin complexes in *trans* could mediate vesicle docking. Syntaxin complexes remained at the sites of docking following detergent solubilization of the lipids. Raised lipid domains could be seen in bilayers containing sphingomyelin, and these domains were devoid of syntaxin and docked vesicles in the presence, but not the absence, of cholesterol. Our results demonstrate that syntaxin is excluded from sphingomyelin-enriched domains in a cholesterol-dependent manner.

Key words: Atomic force microscopy — SNARE — Syntaxin — Lipid bilayer — Lipid microdomain — Membrane

Introduction

SNAREs (soluble *N*-ethylmaleimide-sensitive fusion protein attachment protein receptors) are believed to represent the core of a ubiquitous membrane fusion machine (Jahn & Südhof, 1999; Lin & Scheller, 2000). In the nerve terminal, for example, the three SNARE proteins — synaptobrevin 2 on the membrane of the synaptic vesicle, and syntaxin 1 and SNAP-25 on the presynaptic plasma membrane — form a parallel four-helix bundle, consisting of two helices contributed by SNAP-25 and one each by synaptobrevin and syntaxin (Sutton et al., 1998). The formation of this extremely tight *trans*-SNARE complex is thought to bring the two interacting membranes close together, so that they fuse (Weber et al., 1998). Most of our current understanding of the operation of the SNAREs is based on studies of either soluble SNARE fragments or detergent extracts of biological membranes, and there is little information about the behavior of these proteins in their native lipid environment.

By analogy with viral fusion proteins, with which the SNAREs share several features (Skehel & Wiley, 1998; Jahn & Südhof, 1999; Markovic et al., 2001), it has been suggested that a membrane fusion event is likely to require the assembly of a protein superstructure involving several SNARE complexes (Hua & Scheller, 2001), which might possibly contribute to the structure of the initial fusion pore. Consequently, attempts have been made recently to address the spatial organization of SNAREs in biological membranes. Particular attention has focused on the association of the SNAREs with lipid domains in the plasma membrane. It is well known that different lipids tend to coalesce in model membranes to form microdomains, or 'rafts' (Brown & London, 2000; Dietrich et al., 2000; Samsonov, Mihalyov & Cohen, 2001; Milhiet, Giocondi & Le Grimellec, 2002; Saslowsky et al., 2002), and evidence for the presence of these rafts in biological membranes is growing (Simons & Toomre, 2000; Sprong, van der Sluijs & van Meer, 2001). For example, treatment of membranes with non-ionic detergents leads to the

Correspondence to: J.M. Edwardson; email: jme1000@cam.ac.uk

production of detergent-resistant membrane fragments that are enriched in cholesterol and sphingolipids, and that are believed to represent the biochemical equivalent of rafts (Brown & Rose, 1992; Röper, Corbeil & Huttner, 2000). Furthermore, these detergent-resistant membranes also contain particular proteins, leading to the proposal that proteins can be selectively clustered in rafts in order to facilitate processes such as cellular signaling and protein trafficking (Simons & Toomre, 2000; Sprong et al., 2001). The association of SNAREs with cholesterol-enriched rafts is at present controversial. In the PC12 neuroendocrine cell line, it has been reported that syntaxin and SNAP-25 are found in partially overlapping clusters, which are dispersed on removal of cholesterol (Lang et al., 2002). Interestingly, despite the dependence of syntaxin-patching on the presence of cholesterol, and the direct association of syntaxin with cholesterol, these clusters seem to be distinct from rafts, since syntaxin was soluble in detergent and did not co-patch with known raft markers. The clustering of syntaxin seems to be functionally significant, since secretory vesicles docked preferentially at the cluster sites, and furthermore, cholesterol depletion, using methyl-β-cyclodextrin, caused a significant reduction in the rate of secretion (Lang et al., 2002). In complete contrast, another study on the same cell line has found that all three SNAREs are enriched in detergent-resistant membranes, indicating that they are indeed targeted to rafts (Chamberlain, Burgoyne & Gould, 2002).

In the present study we have used atomic force microscopy to examine the behavior of a single SNARE protein, syntaxin 1, under physiological conditions. We first studied the properties of the free protein, both with and without its transmembrane region (TMR). We then integrated full-length syntaxin into liposomes and used these to produce supported lipid bilayers. We report that syntaxin in lipid bilayers forms complexes that mediate the docking of syntaxin-containing vesicles onto the bilayer. Both, integrated syntaxin complexes and docked vesicles, are efficiently excluded from sphingomyelin-enriched lipid microdomains, provided that cholesterol is also present.

Materials and Methods

Preparation and Analysis of Syntaxin

Rat syntaxin 1A (either full-length (residues 1–288) or lacking the transmembrane region (residues 1–265)) was expressed in the *E. coli* strain DH5α as a glutathione-*S*-transferase- (GST-)fusion protein in the vector pGEX-2T (Amersham Pharmacia Biotech, United Kingdom). GST-syntaxin was purified using glutathione-Sepharose 4B beads (Amersham), according to the manufacturer's instructions. The fusion protein was eluted from the beads in 50 mM HEPES, pH 7.6, 100 mM NaCl (HEPES-buffered saline; HBS), containing 0.5% 3-[(3-cholamidopropyl)dimethylammonio]-1-propanesulfonic acid (CHAPS) and glutathione (normally 10 mM). Where appropriate, the GST tag was removed by incubation with thrombin (Amersham; 100 U/ml for 2.5 h at room temperature). Thrombin was inactivated by addition of phenylmethylsulfonyl fluoride (1 mM), and then removed by adsorption to benzamidine-Sepharose beads (Amersham). Protein quantitation was carried out using a detergent-compatible protein assay kit (BioRad, Hemel Hempstead, United Kingdom). Protein purity was assessed by SDS-polyacrylamide gel electrophoresis (SDS-PAGE), either under non-reducing conditions or after heating under reducing conditions, with Coomassie blue staining.

Syntaxin was further analyzed by continuous sucrose density gradient centrifugation. Syntaxin was layered onto a linear 5–20% sucrose density gradient containing 0.5% CHAPS in HBS (total volume 5 ml), and the gradient was centrifuged at $140{,}000 \times g$ for 18 h at 4°C. Fractions (500 μl) were collected from the top of the gradient, and subjected to SDS-PAGE. Separated proteins were electrophoretically transferred to nitrocellulose (Schleicher & Schuell, Dassel, Germany) by semi-dry blotting. Blots were probed with a mouse monoclonal anti-syntaxin antibody (HPC-1; Barnstable, Hofstein & Akagawa, 1985) at a dilution of 1:1500. Immunoreactive bands were visualized using a horseradish peroxidase-conjugated goat anti-mouse secondary antibody (BioRad; 1:20,000) and enhanced chemiluminescence (Pierce & Warriner, Chester, United Kingdom).

For some experiments, a complex was formed between GST-syntaxin and munc-18, prepared from rat brain. All procedures were carried out at 4°C. Two rat brains were homogenized in HBS, containing a protease inhibitor cocktail (Roche, Mannheim, Germany), and Triton X-100 was added to 2%. After a 30-min incubation, with mixing, the extract was centrifuged at $15{,}000 \times g$ for 30 min. The supernatant was then centrifuged at $140{,}000 \times g$ for 1 h. The second supernatant was incubated with glutathione-Sepharose beads to remove endogenous GST. The extract was then added to GST-tagged full-length syntaxin bound to glutathione-Sepharose, and incubated for 1 h, with mixing. The beads were then washed three times with HBS, containing 0.5% CHAPS. The GST-syntaxin/munc-18 complex was eluted from the beads with 5 mM glutathione, as described above.

Atomic Force Microscopy

Samples were imaged using a Multimode atomic force microscope with a Nanoscope IIIa controller (Digital Instruments, Santa Barbara, CA) equipped with a J-scanner. Oxide-sharpened silicon nitride tips mounted on cantilevers with spring constants of 0.32 N/m were used in intermittent tapping mode. The cantilever oscillation was tuned to a frequency between 8–9 kHz and the drive amplitude was adjusted to produce a root-mean-square amplitude of approximately 0.3–0.5 V. Force was minimized by adjusting the setpoint to just below the jump-off point of the tip. The scan rate was 1 Hz. All scanning was carried out at room temperature (22°C). Images were flattened using the Nanoscope software.

For AFM imaging of syntaxin on mica, 30 μl of protein at a concentration of 0.2 μg/ml in HBS, containing 0.5% CHAPS, was deposited onto muscovite mica (Goodfellow, Cambridge, United Kingdom). The sample was washed three times with 1 ml of HBS/CHAPS and imaged under fluid.

Molecular Volume Calculation

The molecular volume of protein particles was determined from particle dimensions derived from AFM images. The height and radii were measured from multiple cross-sections of the same

particle, and the molecular volume was calculated using the following equation, which treats the particle as a spherical cap

$$V_m = (\pi h/6)(3r^2 + h^2) \quad (1)$$

where h is the particle height and r is the radius (Schneider et al., 1998). Radii were measured at half the particle height to minimize the error introduced by the geometry of the scanning tip (Neish et al., 2002). Molecular volume based on molecular weight was calculated using the equation

$$V_c = (M_0/N_0)(V_1 + dV_2) \quad (2)$$

where M_0 is the molecular mass of the protein, N_0 is Avogadro's number, V_1 and V_2 are the partial specific volumes of protein and water (0.74 cm^3/g and 1 cm^3/g, respectively), and d is the extent of protein hydration (0.4 mol water/mol protein) (Edstrom et al. 1990). Values quoted are means ± SE. Some areas scanned by AFM contained features that were obviously very large aggregates of material (with a radius at least 3-fold greater than the mean value). These aggregates were excluded from calculations of mean particle size.

Integration of Syntaxin into Liposomes

Dioleoylphosphatidylcholine (DOPC), brain sphingomyelin (almost exclusively C18:0) and cholesterol were purchased from Avanti Polar Lipids (Alabaster, AL) and used without further purification. Chloroform solutions of DOPC and sphingomyelin, with or without cholesterol (33 mol%), were dried down under a stream of nitrogen. The lipids were re-hydrated overnight in distilled water to a final concentration of 2 mg/ml. The lipid mixture was vortexed to produce large multi-lamellar vesicles, and small unilamellar vesicles were then produced by mild sonication in a bath sonicator (Decon, Hove, United Kingdom) for 30 min (Reviakine & Brisson, 2000). Syntaxin (5 μl of a 200 μg/ml solution in HBS, containing 0.5% CHAPS) was added to 50 μl of lipid suspension, and sonication was allowed to proceed for a further 30 s. This dilution brought the concentration of CHAPS well below its critical micellar concentration. Protein-free liposomes were produced in the same way, except that syntaxin was omitted.

The extent of syntaxin integration into liposomes was determined by flotation of the liposomes on a discontinuous sucrose density gradient. Samples (500 μl) of liposomes prepared in the presence of syntaxin were added to 1.5 ml of 80% sucrose in HBS. Onto this suspension (now 60% sucrose) was layered 1.5 ml of 50% sucrose in buffer and then 1.5 ml of buffer alone. The gradient was centrifuged at 140,000 × g for 2 h at 4°C. Fractions (500 μl) were taken from the top of the gradient and analyzed by SDS-PAGE and immunoblotting, as above.

Electron Microscopy of Liposomes

Protein-free liposomes prepared from an equimolar mixture of DOPC, sphingomyelin and cholesterol were adsorbed onto glow-discharged 300 mesh copper grids that had been coated with Formvar and carbon, and negatively stained with 1% potassium phosphotungstate at pH 7.0. They were viewed using a Philips CM100 electron microscope operated at 80 kV, using a 50 μm objective aperture. Images were recorded on Kodak SO 143 cut film.

AFM Imaging of Syntaxin in Supported Lipid Bilayers

Supported bilayers were formed by the deposition of 10 μl of vesicle suspension onto mica, immediately followed by 50 μl of HBS, containing 2 mM $CaCl_2$. After a 3-min incubation at room temperature, the sample was gently rinsed with the same buffer and transferred to the atomic force microscope. Protein-free bilayers prepared in this manner were also incubated with 5 μl of syntaxin-containing liposomes for 3 min at room temperature, rinsed and imaged by AFM. AFM imaging was carried out as described above in HBS containing 2 mM $CaCl_2$. Where appropriate, bilayers were stripped by addition of 10 μl of 1% Triton X-100 to the AFM fluid cell (volume 100 μl) during scanning.

Results

The aim of this study was to examine the behavior of syntaxin in lipid bilayers. Since single-molecule analysis of syntaxin under near-physiological conditions had not previously been attempted, we began our study by imaging free syntaxin, in order to gain an understanding of the state in which this protein exists in solution. Recombinant rat syntaxin 1A, either full-length or lacking its transmembrane region (minus-TMR), were prepared as GST-fusion proteins. Where appropriate, the GST tag was removed by thrombin cleavage. As shown in Fig. 1, these procedures resulted in the preparation of purified proteins of the expected molecular masses (60 and 58 kDa for full-length and minus-TMR GST-tagged protein, and 35 and 33 kDa for full-length and minus-TMR untagged protein, respectively). Fig. 1 also shows that untagged full-length syntaxin behaves as a large species under non-reducing conditions, but as a monomer after heating under reducing conditions. In contrast, minus-TMR syntaxin runs as a monomer under both conditions. This result indicates that full-length, but not minus-TMR, syntaxin has a tendency to aggregate, as reported previously (Laage et al., 2000).

The four forms of syntaxin were first imaged bound to mica. The majority (92%) of the particles seen in images of GST-tagged full-length syntaxin was small and globular (Fig. 2*a*). However, 8% of the particles were rosette-like, consisting of a large central core surrounded by a ring of smaller 'petals'. The average number of petals per rosette was five. The rosette structure is more obvious in the gallery of zoomed images shown in Fig. 2*b*. Sections through the particles were used to calculate the molecular volumes of the different features. The distribution of these molecular volumes is shown in Fig. 2*c*. The volume of the small particles was 202 ± 15 nm^3 (n = 30); the volume of the rosette core was 2450 ± 200 nm^3 (n = 30), while the petals had a volume of 237 ± 16 nm^3 (n = 30). Hence, the total molecular volume of an average (5-petal) rosette was 3635 nm^3. Taking into account the numbers and volumes of the particles detected, the rosettes accounted for approximately 60% of the total protein in the sample. The predicted molecular volume for a single GST-syntaxin molecule (molecular mass 60 kDa) is 114 nm^3.

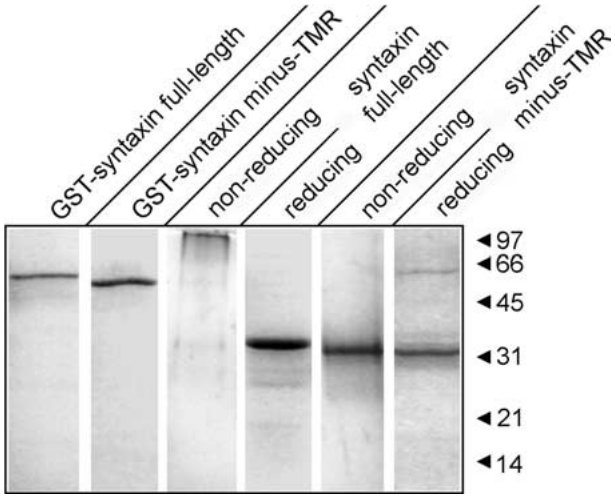

Fig. 1. Purification of syntaxin. Recombinant syntaxin 1A (both full-length and minus-transmembrane region (TMR)) were prepared as GST-fusion proteins. Where appropriate, the GST tag was cleaved using thrombin. Purified proteins (1 μg) were analyzed by either non-reducing or reducing SDS-PAGE, with Coomassie blue staining. Note that untagged full-length syntaxin behaves as a large species under non-reducing conditions, but as a monomer after heating under reducing conditions. In contrast, minus-TMR syntaxin runs as a monomer under both conditions. Molecular mass markers (kDa) are shown on the right.

Hence, the small particles most likely represent dimers, possibly produced by dimerization of the GST tag. A typical rosette must contain approximately 30 protein molecules. This value might in fact be an overestimate, since some of the volume of the particle will be contributed by detergent (CHAPS) bound to the syntaxin TMRs.

When the GST tag was removed from full-length syntaxin, many small particles were again seen; however, the rosette-like structures disappeared (Fig. 2*d*, *e*), leaving large core structures. The mean molecular volume of the particles was 1480 ± 210 nm^3 (n = 93; Fig. 2*f*). Bearing in mind the likely contribution of TMR-bound detergent, this volume corresponds to a maximum of 22 syntaxin molecules of expected molecular volume 66 nm^3. This result indicates that the rosette structure depended on the presence of the GST tag, although the petals are too large to represent single GST molecules. It should also be noted that the broad distribution of molecular volumes (Fig. 2*f*), and the relatively large standard error on the molecular volume for untagged syntaxin (14% of the mean, compared with 8% for GST-syntaxin) reflects a larger range in particle size of the untagged protein, which in turn suggests that it adopts a more heterogeneous structure than the GST-tagged protein. Taken together, these AFM images confirm the propensity of syntaxin containing a TMR to aggregate.

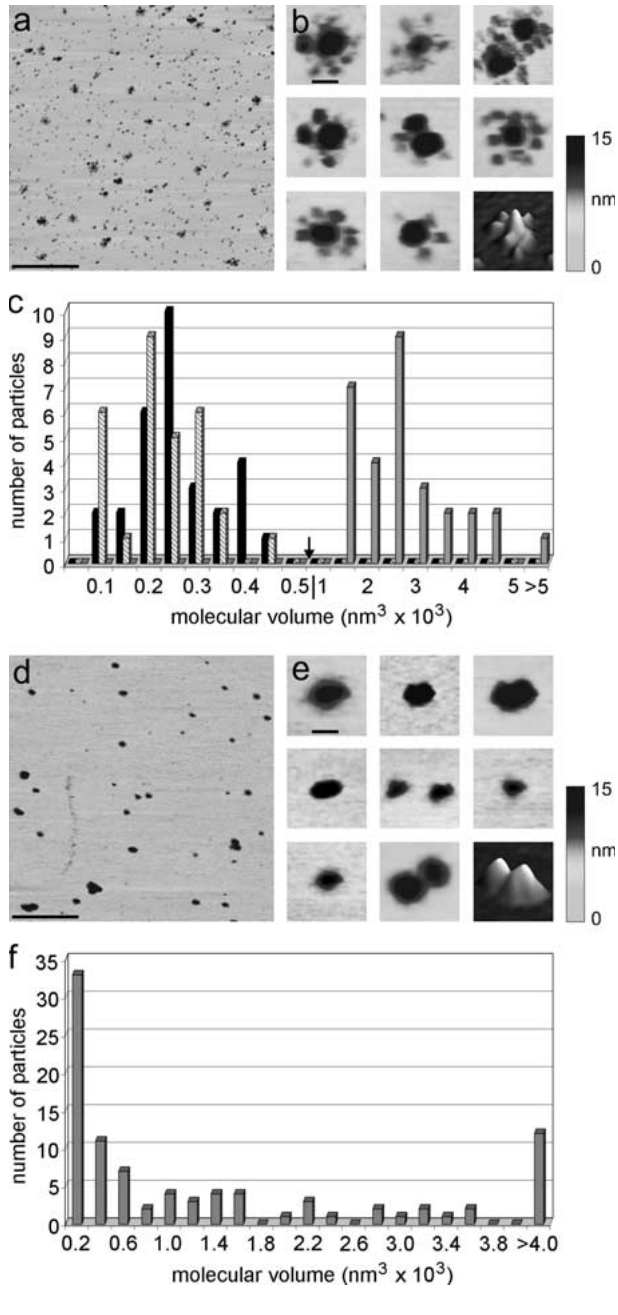

Fig. 2. AFM imaging of full-length syntaxin bound to mica. Proteins were adsorbed onto mica, and imaged under fluid using tapping-mode AFM. (*a*) GST-tagged full-length syntaxin. Note the presence of two types of feature: small, globular particles and larger rosettes. (*b*) Gallery of images of GST-tagged full-length syntaxin, illustrating the structure of the rosette-like particles. (*c*) Distribution of the molecular volumes of the various features seen in images of GST-tagged full-length syntaxin. *Hatched bars:* small particles; *black bars:* rosette petals; *grey bars:* rosette cores. Note that the bin size changes from 50 nm^3 to 500 nm^3 at the point indicated by the arrow. Only alternate bins are labeled. (*d*) Untagged full-length syntaxin. (*e*) Gallery of images of full-length syntaxin. (*f*) Distribution of the molecular volumes of the various features seen in images of untagged full-length syntaxin. Only alternate bins are labeled. Shade-height scales are shown at the right. Scale bars, 500 nm (*a* and *d*), and 33 nm (*b* and *e*).

GST-tagged minus-TMR syntaxin appeared as smaller particles than the full-length form, and no rosettes were visible (Fig. 3*a*, *b*). The molecular volume of these particles (116 ± 8 nm^3, $n = 69$; Fig. 3*c*) was in close agreement with the expected value of 110 nm^3 for a protein of molecular mass 58 kDa, indicating that the particles are monomers. Particles of untagged minus-TMR syntaxin were smaller still (Fig. 3*d*, *e*), and the molecular volume (72 ± 4 nm^3, $n = 79$; Fig. 3*f*) was again consistent with the presence of protein monomers of molecular mass 33 kDa (expected molecular volume 62 nm^3).

The large range in particle size of untagged full-length syntaxin observed by AFM was also apparent in its behavior on a continuous sucrose density gradient. As shown in Fig. 4*a*, syntaxin migrated either at the top or the bottom of the gradient in approximately equal proportion. When samples from fractions 2 and 10 were recentrifuged on identical gradients, some degree of drift in the migration of syntaxin was seen (Fig. 4*b*, *c*); that is, some of the small particles became larger while some of the large aggregates broke up. When fraction 2 was imaged by AFM, the majority of the particles was small, and their molecular volume (164 ± 20 nm^3, $n = 30$) indicated that they consisted on average of 2–3 syntaxin molecules (molecular volume 66 nm^3 for a syntaxin monomer), although some larger particles were seen (Fig. 4*d*). In fraction 10 most of the particles were large (molecular volume 3020 ± 337 nm^3, $n = 30$), although some smaller particles were also present (Fig. 4*e*). The persistence of the two populations of syntaxin during gradient centrifugation indicates that both represent relatively stable structures.

GST-tagged full-length syntaxin was routinely eluted from the glutathione-Sepharose beads by incubation in 10 mM glutathione, according to the manufacturer's instructions. We reasoned that it might be possible to generate samples enriched in syntaxin in different aggregation states by varying the elution conditions. Specifically, we predicted that syntaxin particles anchored by multiple GST tags might be more resistant to elution than syntaxin monomers. Accordingly, we used successive elutions at increasing glutathione concentrations (2, 5, 10 and 15 mM). Fig. 5*a*, *b* show AFM images of samples of GST-syntaxin eluted at 5 mM and 15 mM glutathione, respectively. It is clear that, as expected, elution at 5 mM glutathione yields predominantly small particles (molecular volume 369 ± 25 nm^3 ($n = 30$), equivalent to a maximum of three monomers per particle), whereas large rosettes are clearly visible after elution with 15 mM glutathione (Fig. 2*a*, *b*).

The cytosolic protein munc-18 is known to play a key role in neuronal exocytosis (Yang et al., 2000; Misura, Scheller & Weis, 2000). Biochemical studies have shown that it binds to a 'closed' conformation of syntaxin, thereby controlling its entry into the SNARE complex (Yang et al., 2000; Misura et al., 2000). When bead-attached GST-syntaxin was incubated with a cytosolic extract from rat brain, it specifically recruited munc-18, and elution with 5 mM glutathione yielded complexes of approximately 1:1

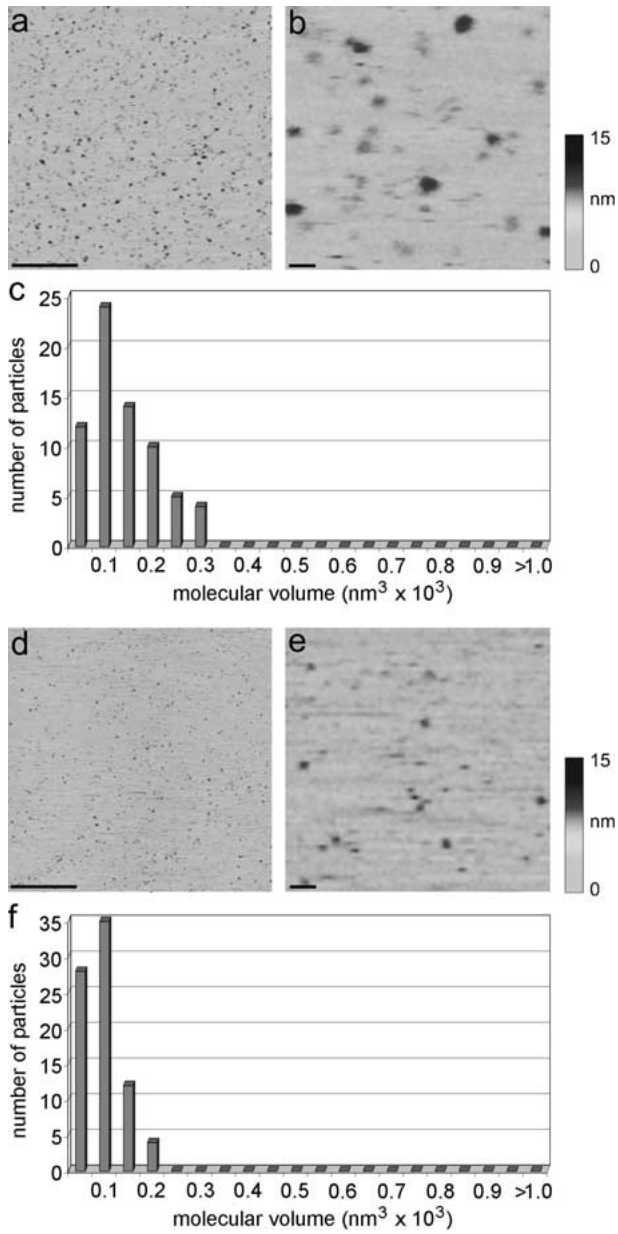

Fig. 3. AFM imaging of minus-TMR syntaxin bound to mica. Proteins were adsorbed onto mica, and imaged under fluid using tapping-mode AFM. (*a*) GST-tagged minus-TMR syntaxin. (*b*) High-magnification view of GST-tagged minus-TMR syntaxin. (*c*) Distribution of the molecular volumes of the various features seen in images of GST-tagged minus-TMR syntaxin. Only alternate bins are labeled. (*d*) Untagged minus-TMR syntaxin. (*e*) High-magnification view of untagged minus-TMR syntaxin. (*f*) Distribution of the molecular volumes of the various features seen in images of untagged minus-TMR syntaxin. Only alternate bins are labeled. Shade-height scales are shown at the right. Scale bars, 500 nm (*a* and *d*), and 33 nm (*b* and *e*).

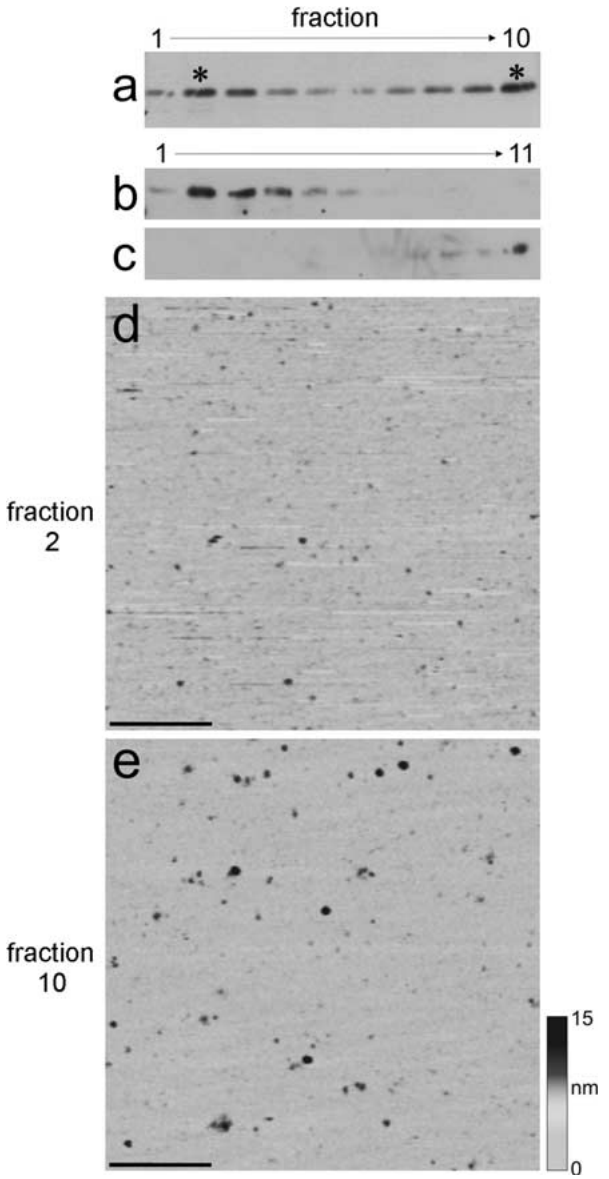

Fig. 4. Visualization of syntaxin in different states of aggregation. (*a*) Purified full-length syntaxin was centrifuged on a linear (5–20%) sucrose density gradient. Fractions (1–10) were collected from the top of the gradient and analyzed by SDS-PAGE followed by immunoblotting using a mouse monoclonal anti-syntaxin antibody. Fractions 2 (*b*) and 10 (*c*) from the gradient shown in (*a*) were re-centrifuged on identical sucrose density gradients, which were analyzed as in (*a*). Fractions 2 (*d*) and 10 (*e*) from the sucrose density gradient in *a* were adsorbed onto mica and imaged under fluid using tapping-mode AFM. A shade-height scale is shown at the right. Scale bars, 500 nm.

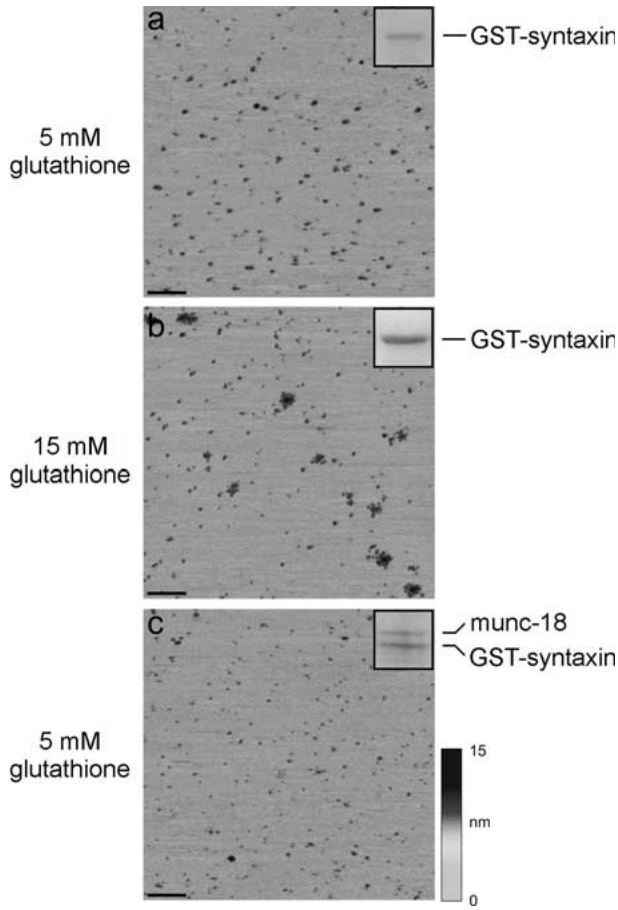

Fig. 5. Manipulation of the aggregation state of syntaxin. GST-tagged full-length syntaxin was eluted from the GSH-Sepharose beads with either 5 mM (*a*) or 15 mM (*b*) glutathione, adsorbed to mica and imaged under fluid using tapping-mode AFM. (*c*) An approximately 1:1 complex of GST-tagged full-length syntaxin and munc-18 was eluted from GSH-Sepharose beads using 5 mM glutathione. The complex was adsorbed onto mica and imaged as in (*a*, *b*). A shade-height scale is shown at the right. Scale bar, 200 nm. Insets show Coomassie-stained protein bands on SDS-polyacrylamide gels.

stoichiometry (Fig. 5c). When the complex was imaged by AFM, the mean molecular volume of the particles detected (177 ± 12 nm^3, $n = 30$) was lower than the predicted volume (246 nm^3) for a 1:1 complex of 60-kDa plus 70-kDa proteins, consistent with the presence of a mixture of single protein molecules and 1:1 complexes. Hence, the binding of munc-18 significantly reduces the degree of aggregation of full-length syntaxin. The larger aggregates seen after elution with 15 mM glutathione (Fig. 5*b*) persisted after incubation with munc-18 (*data not shown*), indicating that these syntaxin complexes are formed before bead-binding.

Initially, we attempted to prepare liposomes containing integrated syntaxin by mixing lipids and protein in the presence of detergent (CHAPS) and then removing the detergent by extensive dialysis. Unfortunately, this method did not result in the successful integration of syntaxin into the liposomes, in agreement with a previous report (Weber et al., 1998). Consequently, we decided to produce unilamellar liposomes first, and then to introduce syntaxin in a small volume of detergent solution, so that the concentration of detergent fell well below its critical

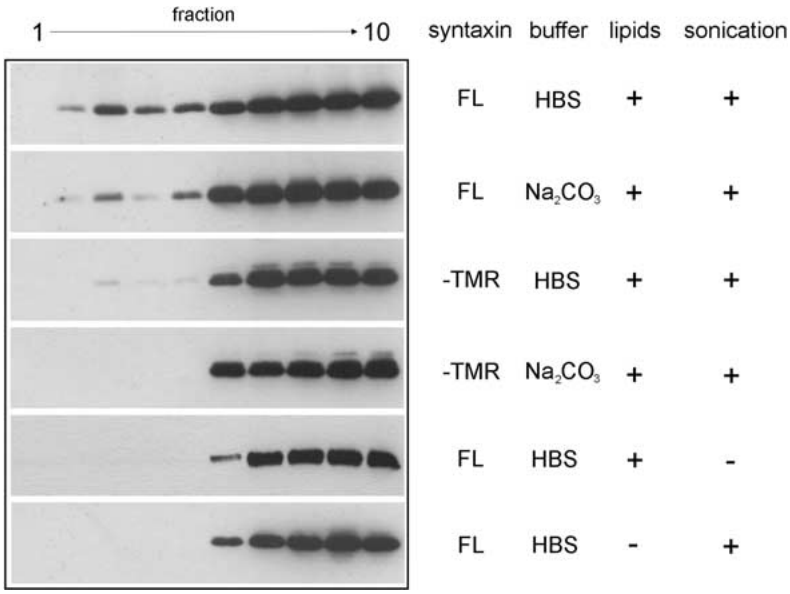

Fig. 6. Integration of syntaxin into liposomes. Lipids (equimolar DOPC, sphingomyelin and cholesterol) were incubated with syntaxin (either full-length or minus-TMR), sonicated briefly and then floated on discontinuous sucrose density gradients. Gradients were prepared in either HBS or Na_2CO_3, as indicated. Fractions (1–10) were taken from the top of the gradients, and syntaxin was detected by SDS-PAGE and immunoblotting using a mouse monoclonal anti-syntaxin antibody. The majority of the lipids were recovered in fractions 2–4 (*data not shown*). In control experiments either the brief sonication or the lipids were omitted.

micellar concentration. To assist integration of the syntaxin, the mixture was subjected to a brief period of sonication using a bath sonicator. The sonication used was very mild, and is unlikely to have had a deleterious effect on the protein. The efficiency of integration of untagged full-length syntaxin into liposomes was determined by discontinuous sucrose density gradient centrifugation. After sonication of an equimolar mixture of DOPC, sphingomyelin and cholesterol in the presence of syntaxin, liposomes were produced that floated above 50% sucrose, to fractions 2–4 of the gradient illustrated in Fig. 6 (*data not shown*; Hodel et al., 2001). Densitometric analysis of the immunoblot showed that 19% of full-length syntaxin migrated into these fractions. When the gradient was prepared in 0.1 M Na_2CO_3, to prevent peripheral association of proteins with the liposomes, the percentage of the syntaxin migrating in fractions 2–4 fell to 8%, which represents the proportion of the added syntaxin that became integrated into the liposomes. A small proportion (1%) of minus-TMR syntaxin floated to fractions 2–4 (Fig. 6); however, this flotation was abolished in Na_2CO_3, indicating that no integration of the minus-TMR protein had occurred. Interestingly, full-length syntaxin did not integrate into the liposomes when the brief sonication step in the presence of both lipids and protein was omitted. Finally, as would be expected, full-length syntaxin did not float in the gradient in the absence of lipids.

When protein-free liposomes containing equimolar DOPC and sphingomyelin were deposited on a mica support and allowed to collapse to form bilayers, raised islands of lipid were evident both in the absence (Fig. 7*a*) and presence (Fig. 7*b*) of cholesterol (33 mol%), as reported previously (Saslowsky et al., 2002).

Sphingomyelin-enriched domains protrude from the surrounding bilayer by 6–9 Å, because the sphingomyelin molecule is longer than the DOPC molecule (Sprong et al., 2001; Saslowsky et al., 2002). When cholesterol-free supported bilayers were produced from liposomes containing equimolar DOPC and sphingomyelin, together with integrated full-length syntaxin, an array of globular features was seen, in addition to the raised lipid domains (Fig. 7*c*). Analysis of the distribution of these features indicated that approximately half were associated with the sphingomyelin-enriched domains (47%; mean of 322 features from 10 images, obtained in four independent experiments). Although the distribution of the features within the sphingomyelin-enriched domains was not studied in detail, inspection of images such as that shown in Fig. 7*c* appeared to show that they tended to sit close to the domain boundaries; however, some of the features were also located close to the centers of the domains. When the bilayer also contained cholesterol (33 mol%), the globular features were again seen, but now they were almost completely (96%; mean of 450 features from 7 images obtained in four independent experiments) excluded from sphingomyelin-enriched domains (Fig. 7*d*). The raised features fell into two categories—a relatively homogeneous population of molecular volume 425 ± 26 nm^3 ($n = 30$), and a more heterogeneous population of larger structures. Most likely, the smaller features represent syntaxin clusters (containing on average six monomers) in the supported bilayer, whereas the large features are vesicles docked onto the bilayer through the formation of syntaxin complexes in *trans*. The section through the scan shown in Fig. 7*d* indicates the dimensions of the major features associated with the bilayer: the height of the sphingomyelin-enriched domain above the back-

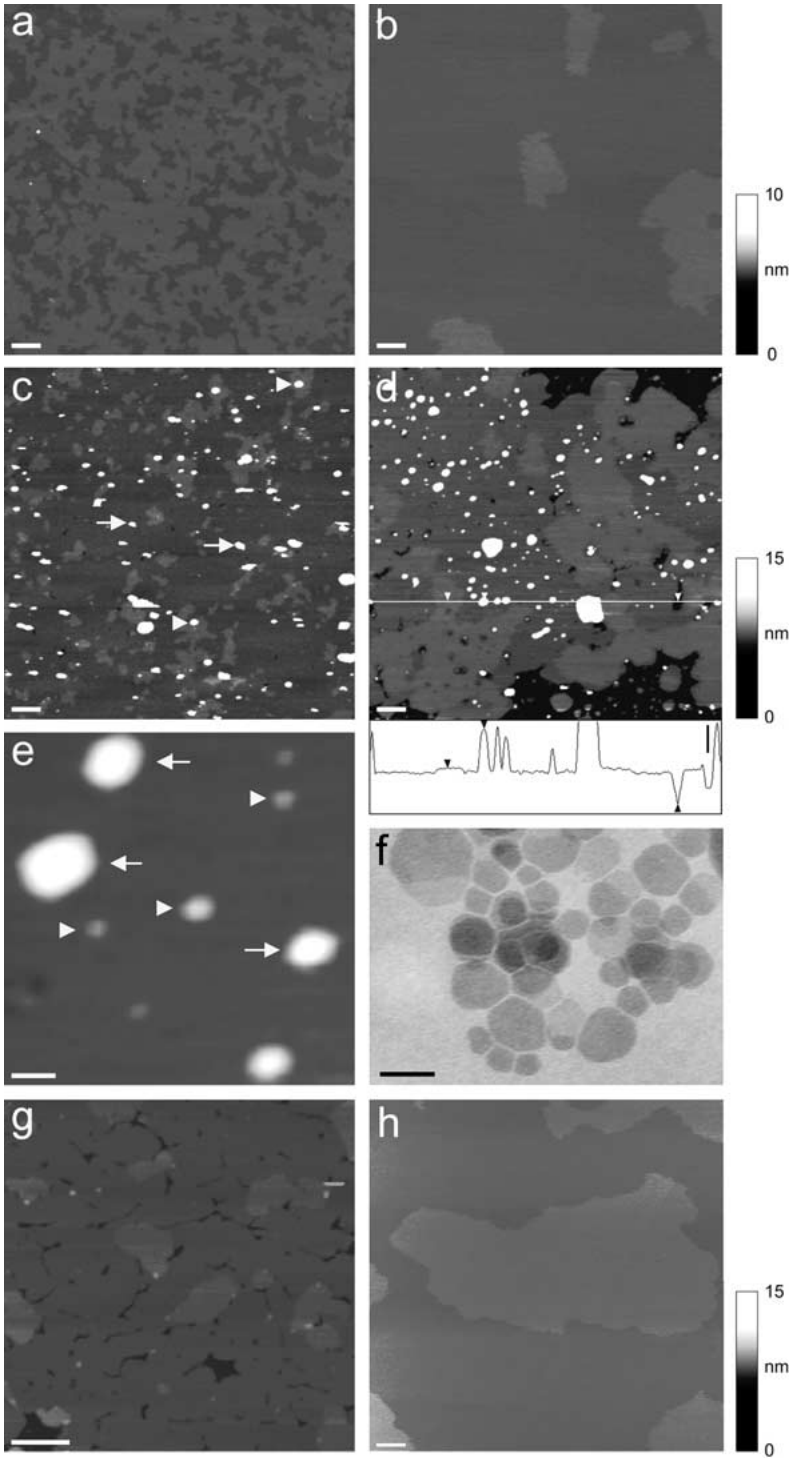

Fig. 7. Exclusion of syntaxin from rafts in supported lipid bilayers. Liposomes were allowed to collapse onto mica, and the resulting bilayers were imaged by AFM using tapping mode under fluid. (*a*) DOPC/sphingomyelin liposomes without syntaxin. (*b*) DOPC/sphingomyelin/cholesterol liposomes without syntaxin. (*c*) DOPC/sphingomyelin liposomes with integrated full-length syntaxin. Arrows and arrowheads indicate syntaxin/vesicles excluded from or located in rafts, respectively. (*d*) DOPC/sphingomyelin/cholesterol liposomes with integrated full-length syntaxin. The vertical section below the panel was taken at the position of the line. Vertical scale bar, 5 nm. Dimensions determined from the scan were as follows: raft height above the background bilayer, 0.7 nm; typical vesicle height, 7.6 nm; typical vesicle diameter at half-height, 48 nm; depth of defect in bilayer, 5.5 nm. (*e*) Higher-magnification image of an area of bilayer containing full-length syntaxin. Arrowheads indicate small features that are likely to be syntaxin clusters; arrows indicate large features that are likely to be docked vesicles. (*f*) Electron micrograph of a sample of liposomes, for comparison with the AFM image in (*e*). (*g*) DOPC/sphingomyelin liposomes pre-incubated with minus-TMR syntaxin. (*h*) Supported bilayer prepared using protein-free DOPC/sphingomyelin/cholesterol liposomes, and then incubated with liposomes containing integrated full-length syntaxin. Note that no liposomes have become attached to the bilayer. Shade-height scales are shown at the right. Scale bars, 250 nm (*a*, *b*, *c*, *d*, *g* and *h*), and 50 nm (*e*, *f*).

ground bilayer was 0.7 nm; a typical vesicle had a height of 7.6 nm, and a half-height diameter of 48 nm; and the depth of a defect in the bilayer was 5.5 nm. Note that the height of the vesicles is considerably less than their diameter, indicating a degree of 'squashing' of the vesicles by the scanning tip. A higher-magnification scan, illustrating the two categories of bilayer-associated particles, is shown in Fig. 7*e*. The electron micrograph (Fig. 7*f*) indicates that the liposomes are predominantly unilamellar, and have a typical diameter of 25–60 nm, consistent with the size of the larger particles found attached to the supported bilayer in the AFM image (Fig. 7*e*). Very few globular features were seen when liposomes were incubated with minus-TMR instead of full-length syntaxin (Fig. 7*g*), indicating that the cytosolic

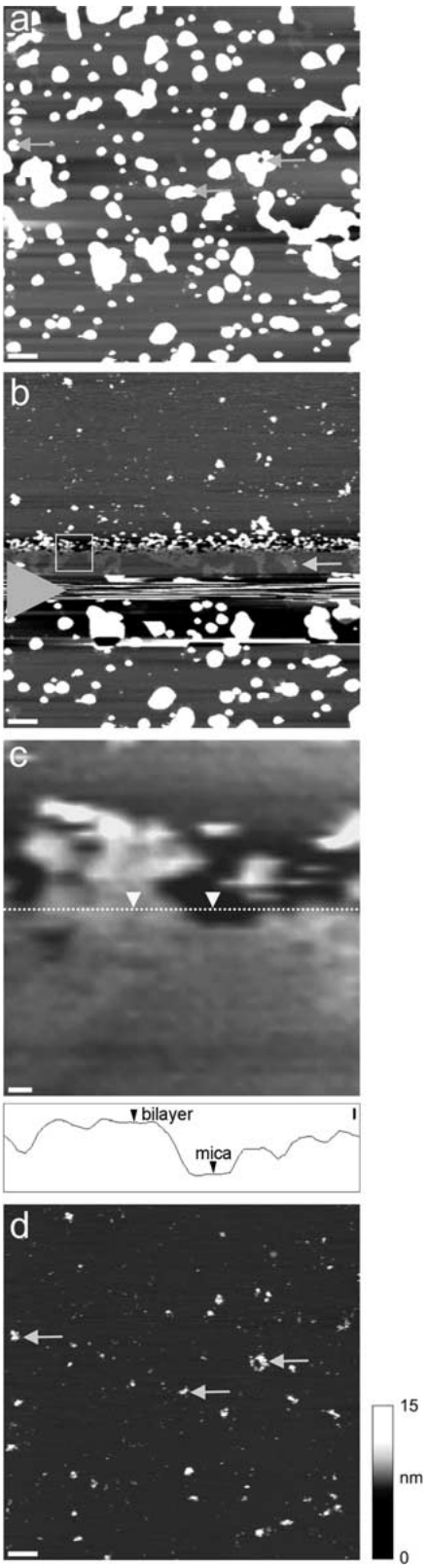

Fig. 8. Co-localization of syntaxin complexes with docked vesicles. DOPC/sphingomyelin liposomes containing full-length syntaxin were allowed to collapse onto mica, and the resulting bilayer was imaged by AFM using tapping mode under fluid. (*a*) Initial scan, showing docked vesicles. (*b*) Scan during which Triton X-100 (0.1%) was added at the point indicated by the arrowhead. (The scan began at the bottom of the image). The arrow indicates rafts at a point just before disintegration of the bilayer. (*c*) Higher-magnification view of the boxed area in (*b*). A vertical section at the position of the dotted line illustrates the difference in height between the bilayer and the mica support (4.8 nm). Arrowheads indicate corresponding positions in the image and the section. (*d*) Subsequent scan of the same area, showing residual syntaxin particles attached to the mica. Arrows indicate points of coincidence between docked vesicles (in *a*) and syntaxin particles (in *d*). A shade-height scale is shown at the bottom right. Horizontal scale bars, 250 nm (*a*, *b* and *d*) and 20 nm (*c*). Vertical scale bar in *c*, 1 nm.

region of syntaxin cannot by itself mediate docking of vesicles onto the supported bilayer. In addition, liposomes containing integrated full-length syntaxin did not attach to pre-formed protein-free bilayers (Fig. 7*h*). Hence, vesicle docking required *trans*-pairing of syntaxin molecules integrated into both vesicles and bilayer.

To investigate further the nature of the raised features seen in bilayers containing syntaxin, and specifically to test whether they do indeed represent docked vesicles, detergent (Triton X-100, final concentration 0.1%) was added to the bilayer during a scan. As shown in Fig. 8, the large globular features docked onto the bilayer rapidly disappeared after detergent addition. After solubilization of the bilayer, a spread of particles remained attached to the mica. These particles closely resembled the structures seen when full-length syntaxin was imaged bound to mica (Fig. 2*b*). Significantly, many of the particles were found in the positions where the putative vesicles had been docked. This result supports our suggestion that the vesicles are docked onto the supported bilayer through the formation of *trans* syntaxin complexes (Fig. 9), and also indicates that the syntaxin in the bilayer must be tightly bound to the mica support. The exclusion of vesicles from the sphingomyelin-enriched domains would then be a consequence of the preferential localization of syntaxin in the DOPC-enriched fluid phase of the supported bilayer. Our data also indicate that this exclusion from sphingomyelin-enriched domains of the bilayer depends on the presence of cholesterol.

Discussion

Our AFM study has revealed dramatic differences in the aggregation states of minus-TMR and full-length syntaxin. Specifically, minus-TMR syntaxin is almost exclusively monomeric, whereas the full-length protein exists in a variety of sizes, from monomers to large multi-molecular aggregates. This tendency of full-length syntaxin to aggregate has already been reported (Laage et al., 2000), although in this previ-

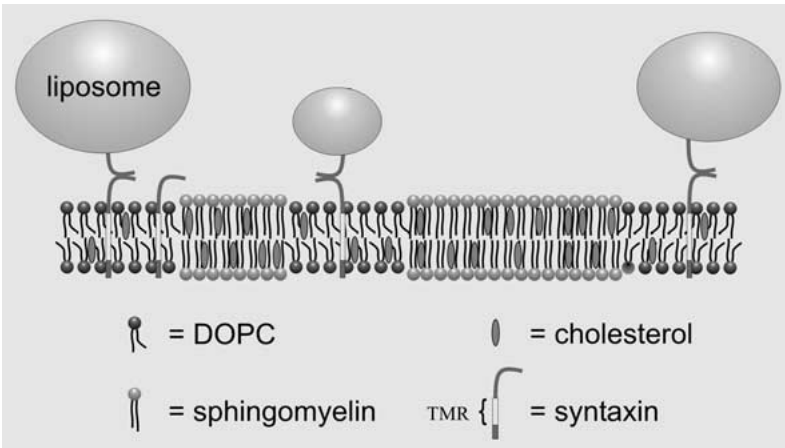

Fig. 9. Model for the behavior of syntaxin in a lipid environment. Rafts contain sphingomyelin and the majority of the cholesterol in the bilayer. Syntaxin is excluded from the rafts, and resides in the DOPC phase of the bilayer. Proteoliposomes are docked to the non-raft regions of the bilayer by syntaxin complexes formed in *trans*.

ous study, the aggregation state of the protein was investigated using 'mild SDS-PAGE', and only dimers were detected. The interactions of syntaxin with its many protein partners (Jahn & Südhof, 1999) have been extensively studied in detergent solutions, and differences have been reported between the binding properties of the minus-TMR and full-length protein. For instance, bead-bound GST-syntaxin was shown to bind efficiently, via its cytoplasmic domain, to synaptotagmin, α/β-SNAP and synaptobrevin, and truncations or deletions of the TMR significantly reduced binding (Lewis et al., 2001). We suggest that at least some of these TMR-dependent interactions might involve the production of syntaxin aggregates, which are likely to have different binding characteristics from the monomeric protein.

An inhibitory effect of munc-18 on the aggregation of full-length syntaxin was clearly demonstrated in our study. This effect may well be replicated in the neuron, where munc-18 is known to act as a molecular chaperone for syntaxin (Yang et al., 2000; Misura et al., 2000). We hoped to be able to exploit the anti-aggregatory effect of munc-18 to insert syntaxin monomers into the lipid bilayers. However, the syntaxin-munc-18 complexes appeared relatively unstable, and the images obtained after bilayer insertion were indistinguishable from those given by syntaxin alone (*data not shown*).

Syntaxin-containing lipid bilayers were found to contain two types of features—protein molecules (probably aggregates) and attached vesicles. No vesicles were seen either when liposomes were prepared in the presence of minus-TMR syntaxin or when liposomes containing integrated full-length syntaxin were added to a pre-formed protein-free supported bilayer. Hence, the vesicles must have docked through the formation of syntaxin complexes in *trans*. The principal aim of this study was to examine the sorting of syntaxin between domains in bilayers containing mixtures of lipids. We found that syntaxin was efficiently excluded from sphingomyelin-rich domains, provided cholesterol was also present. This behavior is the reverse of that shown by the glycosylphosphatidylinositol-anchored protein placental alkaline phosphatase, which we have shown recently is almost exclusively targeted into sphingomyelin-enriched domains, but in a cholesterol-independent manner (Saslowsky et al., 2002). The results of the present study are largely in agreement with those of Lang et al. (2002), who found that syntaxin was clustered in a cholesterol-dependent manner in the plasma membranes of PC12 cells, but that the protein was excluded from rafts. In contrast, Chamberlain et al. (2002) reported that all three SNAREs are raft-associated in PC12 cell membranes. In neurons, both syntaxin and SNAP-25 are found throughout the axonal plasma membrane and not just at the nerve terminal, where exocytotic membrane fusion occurs (Garcia et al., 1995). Furthermore, the patching of syntaxin and SNAP-25 in the PC12 cell plasma membrane has been shown to be overlapping but not coincident (Lang et al., 2002). It is possible, therefore, that the different SNAREs interact closely only when the SNARE complex is being formed. Why the two studies on PC12 cells should have produced such discrepant results, however, is at present unclear.

What would be the advantage of clustering syntaxin in a sub-domain of the plasma membrane? It is well established that syntaxin and SNAP-25 combine with the synaptic vesicle protein synaptobrevin to form the SNARE complex, which is a key component of the membrane fusion machine. Viral membrane fusion shows striking similarities with SNARE-mediated fusion. For instance, both require the formation of stable helical bundles, and both involve conformational changes that cause close membrane apposition. Influenza hemagglutinin, a model viral fusion protein, is a homotrimer (Skehel & Wiley, 1998), and it has recently been shown that the efficiency of its low pH-triggered conformational change depends on the density of hemagglutinin molecules in

the membrane (Markovic et al., 2001). It was proposed that this concerted activation of adjacent proteins might represent the mechanism by which a group of fusion proteins coordinate their activity at the fusion site. The similarities between the viral proteins and the SNAREs suggest that SNARE-mediated fusion might also involve the action of a number of SNARE complexes. In fact, evidence has recently been presented that three SNARE complexes act together to trigger a membrane fusion event in PC 12 cells (Hua & Scheller, 2001). The clustering of the SNARE proteins into particular membrane domains might therefore increase the likelihood that a number of *trans*-SNARE complexes could form in close proximity, thereby increasing the probability of a membrane fusion event.

The detergent solubility of influenza hemagglutinin falls as the protein migrates through the secretory pathway towards the plasma membrane, consistent with its recruitment into rafts (Skibbens, Roth & Matlin, 1989). This raft association appears to be involved in the delivery of the protein specifically to the apical surface of polarized epithelial cells (Prydz & Simons, 2002). The non-neuronal syntaxin isoform, syntaxin 3, has also been shown to be enriched in a Triton X-100-insoluble membrane fraction from Madin-Darby canine kidney cells (Lafont et al., 1999), and in a Lubrol-insoluble fraction of pancreatic zymogen granules (Kalus et al., 2002). In both cell types, this syntaxin isoform is apically targeted, suggesting that here, too, the purpose of raft association is to ensure correct intracellular sorting of the protein. The C-terminal tail of hemagglutinin contains three cysteine residues. All three of these residues are normally palmitoylated (Naim et al., 1992), and mutation of any one of these residues almost abolishes raft association (Melkonian et al., 1999), but has no effect on membrane fusion, indicating that raft association is not required for fusion. There is also evidence for the requirement for sphingolipids and cholesterol in the target membrane for viral membrane fusion; furthermore, the ectodomain of the Semliki Forest virus fusion protein E1 associates with sterol-rich domains (Ann, Gibbins & Kielian, 2002). Nevertheless, there appears to be no requirement for the presence of rafts in the target membrane for membrane fusion, since Semliki Forest virus, for example, fuses with liposomes irrespective of the presence or absence of Triton X-100-insoluble microdomains (Waarts, Bittman & Wilschut, 2002). In PC12 cells, depletion of cholesterol, using methyl-β-cyclodextrin, causes a reduction in the efficiency of exocytotic membrane fusion (Lang et al., 2002). Although membrane rafts are likely to be dispersed by this treatment, it is possible that the inhibition of syntaxin clustering is the prime cause of the functional effect. The requirement for sterols in membrane fusion extends to yeast. Here, ergosterol is required at the priming stage of homotypic fusion between yeast vacuoles (Kato & Wickner, 2001). Clearly, then, sterols are required for a variety of very different membrane fusion events. However, the actual involvement of rafts in these fusion events, and the arrangement of SNARE proteins with respect to the rafts, still needs to be elucidated. In fact, a sterol-dependent exclusion of SNAREs from the more ordered raft domains, and their consequent clustering in the more fluid non-raft region of the membrane, might actually be conducive to fusion.

We are grateful to Dr. J. Skepper (Multi-Imaging Laboratory, Department of Anatomy, University of Cambridge, United Kingdom) for expert assistance with the electron microscopy, and to Dr. B. Davletov (MRC Laboratory of Molecular Biology, Cambridge, United Kingdom) for many helpful discussions, and for critical reading of this manuscript. This work was supported by Grant B12816 from the Biotechnology and Biological Sciences Research Council (to R.M.H. and J.M.E.). J.C.L. was supported by an Overseas Research Scholarship and the Cambridge Commonwealth Trust.

References

Ahn, A., Gibbons, D.L., Kielian, M. 2002. The fusion peptide of Semliki Forest virus associates with sterol-rich membrane domains. *J. Virol.* **76**:3267–3275

Barnstable, C.J., Hofstein, R., Akagawa, K. 1985. A marker of early amacrine cell development in rat retina. *Dev. Brain Res.* **20:**286–290

Brown, D.A., London, E. 2000. Structure and function of sphingolipid- and cholesterol-rich membrane rafts. *J. Biol. Chem.* **275:**17221–17224

Brown, D.A., Rose, J.K. 1992. Sorting of GPI-anchored proteins to glycolipid-enriched membrane subdomains during transport to the apical cell surface. *Cell* **68:**533–544

Chamberlain, L.H., Burgoyne, R.D., Gould, G.W. 2002. SNARE proteins are highly enriched in lipid rafts in PC12 cells: implications for the spatial control of exocytosis. *Proc. Natl. Acad. Sci. USA* **98:**5619–5624

Dietrich, C., Bagatolli, L.A., Volovyk, Z.N., Thompson, N.L., Levi, M., Jacobson, K., Gratton, E. 2000. Lipid rafts reconstituted in model membranes. *Biophys. J.* **80:**1417–1428

Edstrom, R.D., Meinke, M.H., Yang, X.R., Yang, R., Elings, V., Evans, D.F. 1990. Direct visualization of phosphorylase-phosphorylase kinase complexes by scanning tunneling and atomic force microscopy. *Biophys. J.* **58:**1437–1448

Garcia, E.P., McPherson, P.S., Chilcote, T.J., Takei, K., DeCamilli, P. 1995. rbSec1A and B colocalize with syntaxin 1 and SNAP-25 throughout the axon, but are not in a stable complex with syntaxin. *J. Cell Biol.* **129:**105–120

Hodel, A., An, S.J., Hansen, N.J., Lawrence, J., Wäsle, B., Schrader, M., Edwardson, J.M. 2001. Cholesterol-dependent interaction of syncollin with the membrane of the pancreatic zymogen granule. *Biochem. J.* **356:**843–850

Hua, Y., Scheller, R.H. 2001. Three SNARE complexes cooperate to mediate membrane fusion. *Proc. Natl. Acad. Sci. USA* **98:** 8065–8070

Jahn, R., Südhof, T.C. 1999. Membrane fusion and exocytosis. *Annu. Rev. Biochem.* **68:**863–911

Kalus, I., Hodel, A., Koch, A., Kleene, R., Edwardson, J.M., Schrader, M. 2002. Interaction of syncollin with GP-2, the major membrane protein of pancreatic zymogen granules, and association with lipid microdomains. *Biochem. J.* **362:**433–442

Kato, M., Wickner, W. 2001. Ergosterol is required for the Sec18/ATP-dependent priming step of homotypic vacuole fusion. *EMBO J.* **20:**4035–4040

Laage, R., Rohde, J., Brosig, B., Langosch, D. 2000. A conserved membrane-spanning amino acid motif drives homomeric and supports heteromeric assembly of presynaptic SNARE proteins. *J. Biol. Chem.* **275:**17481–17487

Lafont, F., Verkade, P., Galli, T., Wimmer, C., Louvard, D., Simons, K. 1999. Raft association of SNAP receptors acting in apical trafficking in Madin-Darby canine kidney cells. *Proc. Natl. Acad. Sci. USA* **96:**3734–3738

Lang, T., Bruns, D., Wenzel, D., Riedel, D., Holroyd, P., Thiele, C., Jahn, R. 2002. SNAREs are concentrated in cholesterol-dependent clusters that define docking and fusion sites for exocytosis. *EMBO J.* **20:**2202–2213

Lewis, J.L., Dong, M., Earles, C.A., Chapman, E.R. 2001. The transmembrane domain of syntaxin 1A is critical for cytoplasmic domain protein-protein interactions. *J. Biol. Chem.* **276:**15458–15465

Lin, R.C., Scheller, R.H. 2000. Mechanisms of synaptic vesicle exocytosis. *Annu. Rev. Cell Dev. Biol.* **16:**19–49

Markovic, I., Leikina, E., Zhukovsky, M., Zimmerberg, J., Chernomordik, L.V. 2001. Synchronized activation and refolding of influenza hemagglutinin in multimeric fusion machines. *J. Cell Biol.* **155:**833–843

Melkonian, K.A., Ostermeyer, A.G., Chen, J.Z., Roth, M.G., Brown, D.A. 1999. Role of lipid modifications in targeting proteins to detergent-resistant membrane rafts. *J. Biol. Chem.* **274:**3910–3917

Milhiet, P.E., Giocondi, M.-C., Le Grimellec, C. 2002. Cholesterol is not critical for the existence of microdomains in kidney brush-border membrane models. *J. Biol. Chem.* **277:**875–878

Misura, K.M.S., Scheller, R.H., Weis, W.I. 2000. Three-dimensional structure of the neuonal-Sec1-syntaxin 1a complex. *Nature* **404:**355–362

Naim, H.Y., Amarneh, B., Ktistakis, N.T., Roth, M.G. 1992. Effects of altering palmitylation sites on biosynthesis and function of the influenza virus hemagglutinin. *J. Virol.* **66:**7585–7588

Neish, C.S., Martin, I.L., Henderson, R.M., Edwardson, J.M. 2002. Direct visualization of ligand-protein interactions using atomic force microscopy. *Brit. J. Pharmacol.* **135:**1943–1950

Prydz, K., Simons, K. 2002. Cholesterol depletion reduces apical transport capacity in epithelial Madin-Darby canine kidney cells. *Biochem. J.* **357:**11–15

Reviakine, I., Brisson, A. 2000. Formation of supported phospholipid bilayers from unilamellar vesicles investigated by atomic force microscopy. *Langmuir* **16:**1806–1815

Röper, K., Corbeil, D., Huttner, W.B. 2000. Retention of prominin in microvilli reveals distinct cholesterol-based lipid microdomains in the apical plasma membrane. *Nature Cell Biol.* **2:**582–592

Samsonov, A.V., Mihalyov, I., Cohen, F. 2001. Characterization of cholesterol-sphingomyelin domains and their dynamics in bilayer membranes. *Biophys. J.* **81:**1486–1500

Saslowsky, D.E., Lawrence, J., Ren, X., Brown, D.A., Henderson, R.M., Edwardson, J.M. 2002. Placental alkaline phosphatase is efficiently targeted to rafts in supported lipid bilayers. *J. Biol. Chem.* **277:**26966–26970

Schneider, S.W., Lärmer, J., Henderson, R.M., Oberleithner, H. 1998. Molecular weights of individual proteins correlate with molecular volumes measured by atomic force microscopy. *Pfluegers Arch.* **435:**362–367

Simons, K., Toomre, D. 2000. Lipid rafts and signal transduction. *Nature Rev. Mol. Cell Biol.* **1:**31–39

Skehel, J.J., Wiley, D.C. 1998. Coiled coils in both intracellular vesicle and viral membrane fusion. *Cell* **95:**871–874

Skibbens, J.E., Roth, M.G., Matlin, K.S. 1989. Differential extractability of influenza virus hemagglutinin during intracellular transport in polarized epithelial cells and nonpolar fibroblasts *J. Cell Biol* **108:**821–832

Sprong, H., van der Sluijs, P., van Meer, G. 2001. How proteins move lipids and lipids move proteins. *Nature Rev. Mol. Cell Biol.* **2:**504–513

Sutton, R.B., Fasshauer, D., Jahn, R., Brunger, A.T. 1998. Crystal structure of a SNARE complex involved in synaptic exocytosis at 2.4Å resolution. *Nature* **395:**347–353

Waarts, B.-L., Bittman, R., Wilschut, J. 2002. Sphingolipid- and cholesterol-dependence of alphavirus membrane fusion. *J. Biol. Chem.* **277:**38141–38147

Weber, T., Zemelman, B.V., McNew, J.A., Westermann, B., Gmachl, M., Parlati, F., Söllner, T.H., Rothman, J.E. 1998. SNAREpins: minimal machinery for membrane fusion. *Cell* **92:**759–772

Yang, B., Steegmaier, M., Gonazalez, L.C. Jr., Scheller, R.H. 2000. nSec1 binds to a closed conformation of syntaxin1A. *J. Cell Biol.* **148:**247–252